

Full paper

Nitrogen-enriched pseudographitic anode derived from silk cocoon with tunable flexibility for microbial fuel cells



Min Lu^{a,1}, Yijun Qian^{a,1}, Cuicui Yang^a, Xiao Huang^a, Hai Li^a, Xiaoji Xie^{a,*}, Ling Huang^{a,*}, Wei Huang^{a,b,**}

^a Key Laboratory of Flexible Electronics (KLOFE), Institute of Advanced Materials (IAM), Jiangsu National Synergetic Innovation Center for Advanced Materials (SICAM), Nanjing Tech University (NanjingTech), Nanjing 211816, PR China

^b Key Laboratory for Organic Electronics and Information Displays, Jiangsu National Synergetic Innovation Center for Advanced Materials (SICAM), Nanjing University of Posts & Telecommunications, Nanjing 210023, PR China

ARTICLE INFO

Keywords:

Silk cocoon
Carbonization
Flexible carbon fiber
Nitrogen-containing functional groups
Microbial fuel cell

ABSTRACT

Microbial fuel cells (MFCs), promising for converting biomass energy into electricity, have attracted much research enthusiasm. However, high performance anode materials for MFC, particularly with tunable flexibility for diverse cell configurations, are still limited. In this study, through a simple one-step carbonization of a versatile protein precursor, silk cocoon, both freestanding and flexible bioanode materials, with enriched nitrogen contents and hierarchical pores, can be easily fabricated. Importantly, the carbonized silk cocoon, as a freestanding MFC anode, and flexible carbon fiber, as a flexible MFC anode, exhibit high performance in electricity generation, yielding about 2.5-fold and 3.1-fold maximum gravimetric power density than that of MFCs with carbon cloth anode, respectively. We attribute the improved anode performance of these flexibility tunable carbon materials to their good biocompatibility, reduced electron transfer resistance and high capacitance. This study will not only offer great opportunities for the fabrication of high-performance MFC anode with varied designs and 3-dimensional architectures, but also shed light on the future development of MFC and proper utilization of the abundant “green” natural resources.

1. Introduction

Microbial fuel cell (MFC), a device harnessing exoelectrogens to harvest electricity from biomass energy, has drawn continuous attention, owing to its ability of simultaneous electricity generation and wastewater treatment [1–3]. In a typical MFC, the anode accommodates exoelectrogens, degrades organic matters and generates electrons [4–6]. An ideal anode should be highly biocompatible and facile for electron generation, together with low cost and long durability. Among various anode candidates, carbon-based anodes give promising potential for further applications, due to the relatively good biocompatibility, high flexibility for manipulation and wide accessibility, and thus have received plenty of research enthusiasm [7,8]. Carbon cloth, as a typical example of carbon-based anodes, is commonly regarded as benchmark for the evaluation of newly developed MFC anodes [9–11]. Nevertheless, currently, the performance of carbon-based anodes is still far beyond expectation, which has severely restricted the wide

application and industrialization of MFC [12,13].

To improve the performance of carbon-based anodes for MFC, three strategies, including improving biocompatibility of anode, providing sufficient space for exoelectrogens and facilitating electron transfer between bacteria and electrode, can be generally adopted through diverse anode manipulation [14]. Recently, three dimensional (3D) carbon-based anodes, following these strategies, have emerged as a new generation of high-performance anodes for MFCs, due to their superior anode performance over traditional ones [15–18]. These 3D anodes can coherently enlarge bacterium-anode interaction area and enhance electron transfer between the bacteria and anode, which exhibit synergetic effects. For example, MFCs, equipped with 3D graphene/Pt composites as anode, can give more than 5-time higher maximum power density when compared with those utilizing carbon cloth [19]. Alternatively, cellulose-based natural materials can derive high performance anodes, which inherit the original 3D macrostructure, but typically don't allow adjustment to macrostructure or

* Corresponding authors.

** Corresponding author at: Key Laboratory of Flexible Electronics (KLOFE), Institute of Advanced Materials (IAM), Jiangsu National Synergetic Innovation Center for Advanced Materials (SICAM), Nanjing Tech University (NanjingTech), Nanjing 211816, PR China.

E-mail addresses: iamxjxie@njtech.edu.cn (X. Xie), iamluhuang@njtech.edu.cn (L. Huang), iamwhuang@njtech.edu.cn (W. Huang).

¹ These authors contributed equally to this work.

mechanical property [16,20]. Apart from the structure manipulation, anode modifications, particularly introduction of nitrogen-containing groups, are typically applied to improve the biocompatibility of anodes, e.g. by NH_3 -assisted heat treatment [21], heterocycle-polymer modification [20], and NH_4HCO_3 pretreatment [22]. It was demonstrated that N-containing functional groups would induce absorption and growth of preferred microbes on the electrode to increase biocatalytic activity, facilitate the extracellular electron transfer, and consequently improve MFC performance [20]. Despite these advances, fabrication of the artificial 3D anodes, along with the sequential modification process to insert N-containing functional groups, is usually time-consuming, complicated and costly. Preparation of nitrogen-enriched 3D anodes in one single step should simplify the construction of MFC anode and thus facilitate the further development of MFC.

Silk cocoon (*Bombyx mori*), one of the most abundant natural polymer composites, owns high nitrogen content (~15%) and intrinsically 3D nonwoven structure with multiple layers and pores [23–25]. Different from cross-linked structure in cellulose-based natural materials, the delicate 3D structure is assembled by random arrangement of one single silk fiber and fixed by sericin—the outmost protein of silk fiber-gelation. When sericin is simply removed by degumming, the mechanical property of silk cocoon can be easily tuned, creating flexible silk fibers. All of these unique features make silk cocoon a suitable candidate for electrochemical device fabrication [18,24–28].

Inspired by the above facts, we here demonstrate that both freestanding and flexible MFC anodes, with nitrogen-enriched and 3D pseudographitic structure, can be obtained by simple preparation methods. After incorporated into a single-chamber MFC reactor, the carbonized silk cocoon anode exhibited improved biocompatibility and performance when compared to those of its counterpart carbon cloth (~2.5 fold in maximum gravimetric power density). Importantly, flexible carbon fibers prepared with an additional degumming procedure, once equipped into a single-chamber MFC as an anode, gave ~1.2 fold maximum power density than that of a directly carbonized silk cocoon anode. These results imply that naturally structured protein, such as silk cocoon, can be a versatile material for carbon-based anode fabrication, which should shed light on the MFC development and applications.

2. Experimental section

2.1. Preparation of carbonized silk cocoon and flexible carbon fiber

Carbonized silk cocoons were obtained by directly heating *Bombyx mori* silk cocoons at 900 °C for 3 h under N_2 flow without any pretreatment and posttreatment. Notably, the pupa was removed in advance from a small opening on silk cocoon.

To obtain flexible carbon fibers, silk cocoons were firstly degummed in boiling Na_2CO_3 solution (500 mg/L) for 20 min, washed by water and dried at 60 °C for overnight. Subsequently, the degummed silk cocoons (flexible silk fibers) were carbonized at 900 °C for 3 h under N_2 flow, resulting in flexible carbon fibers.

2.2. Material characterization

The Raman spectra were collected on a confocal microscope Raman spectrometer system (Witec Alpha 300). Powder X-ray diffraction measurement was carried out on an ARL X'TRA diffractometer with graphite monochromatized Cu K α radiation. Thermogravimetric analysis (TGA) was performed on a Netzsch STA-499 F3 at argon atmosphere. Vario EL III (Elementar) was used for elemental analysis. X-ray photoelectron spectroscopy (XPS, PHI 5000 VersaProbe) was employed to examine the functional groups. Brunauer-Emmett-Teller (BET) specific surface area and pore size of the materials were measured by an ASAP 2460 analyzer (Micromeritics). Scanning electron microscope (SEM) analysis was performed on a scanning

electron microscope (HITACHI, S-4800). To obtain SEM images of anode samples attached with biofilm, the samples were firstly immersed into glutaraldehyde solution (3 wt%, 0.5 h), followed by washing three times with 0.2 M phosphate buffer saline (pH 6.8). The samples were then dehydrated stepwise in a series of ethanol/water solutions (ethanol concentration: 50%, 70%, 80%, 90%, and 100%) and dried in a desiccator prior to SEM analysis.

2.3. Microbial fuel cell (MFC) setup and operation

Single-chamber MFCs, with air cathode and cylindrical chamber (diameter: 3.0 cm, length: 4.0 cm and volume: 28 mL), were constructed by using plexiglass. To fabricate MFC air cathode, the carbon cloth (30% wet proof, Hesen, Shanghai, China) was coated with 20% polytetrafluoroethylene (PTFE, DuPont, USA) and annealed at 370 °C for 30 min to make a gas diffusion layer (PTFE loading amount ~10 mg/cm²). Subsequently, an ethanol solution (1 mL), containing 15 mg platinum/carbon black (Pt: 20 wt%, Johnson Matthey, USA) and 105 μL 2 wt% PTFE, was coated onto the opposite side of carbon cloth, and annealed at 370 °C for 30 min, forming a catalyst layer [29]. The resulting carbon cloth based cathode contained ~0.8 mg/cm² Pt catalyst. Carbonized silk cocoon based MFC anodes were obtained by directly stringing one, two or three carbonized silk cocoons with titanium wire, while flexible carbon fiber based MFC anodes were assembled by twisting titanium wire with the carbon fibers. Hydrophilic carbon cloth (Hesen, Shanghai, China) was used as the MFC anode to fabricate control cells. Each anode was tested in duplicate.

The fabricated MFCs were inoculated with 15.0 mL of preacclimated bacteria originally from activated anaerobic sludge. These MFCs were then operated in batch mode at 30 ± 4 °C for inoculation [30] and fed on artificial wastewater. The artificial wastewater was a mixture of CH_3COONa (1 g/L), $\text{NaH}_2\text{PO}_4 \cdot 2\text{H}_2\text{O}$ (2.46 g/L), Na_2HPO_4 (4.57 g/L), NH_4Cl (0.31 g/L), KCl (0.13 g/L), vitamin stock solution (5 mL/L), and mineral stock solution (12.5 mL/L) [31]. Fresh artificial wastewater was refilled when the voltage dropped below 0.05 V with an external resistor of 1000 Ω .

2.4. Electrochemical measurement

The close circuit voltage of MFCs was recorded, over a 1000 Ω external resistor, by a data acquisition system (Yavii YAV, 16 channels, Wuhan, China). Polarization curves were obtained by linear sweep voltammetry (scanning rates: 0.1 mV/s), using a CHI 630E electrochemical work station (Chenhua Instruments Co. Ltd., Shanghai, China), with 2-electrode setup (working electrode: MFC cathode, counter electrode and reference electrode: MFC anode). Cyclic voltammograms at both turnover and non-turnover conditions were implemented with scanning rates of 1 mV/s and potential range of -0.6–0.2 V in 3-electrode mode (working electrode: MFC anode, counter electrode: MFC cathode and reference electrode: Ag/AgCl, 3 M KCl). Turnover state was created by running a MFC at close circuit over an external resistor of 1000 Ω after refilling fresh artificial wastewater, until stable voltage output was achieved. Non-turnover state was created by running a MFC for 36 h without refilling artificial wastewater, and prior to cyclic voltammetric test, the MFC was refilled with phosphate buffer saline (50 mM) and degassed by argon. For self-charging/discharging measurement, MFCs with freshly filled artificial wastewater were stabilized at open circuit. The MFCs were then self-charged at open circuit for 1200 s, followed by discharging at a fixed anode potential of -0.35 V (vs. Ag/AgCl, 3 M KCl) for 1200 s. Electrochemical impedance spectroscopy was carried out at stable open circuit condition using a PGSTAT 302N (Autolab) in the frequency range of 100000–100 mHz (amplitude: 5 mV) at 3-electrode mode (working electrode: MFC anode, counter electrode: MFC cathode and reference electrode: Ag/AgCl, 3 M KCl). The results were plotted as Nyquist plots

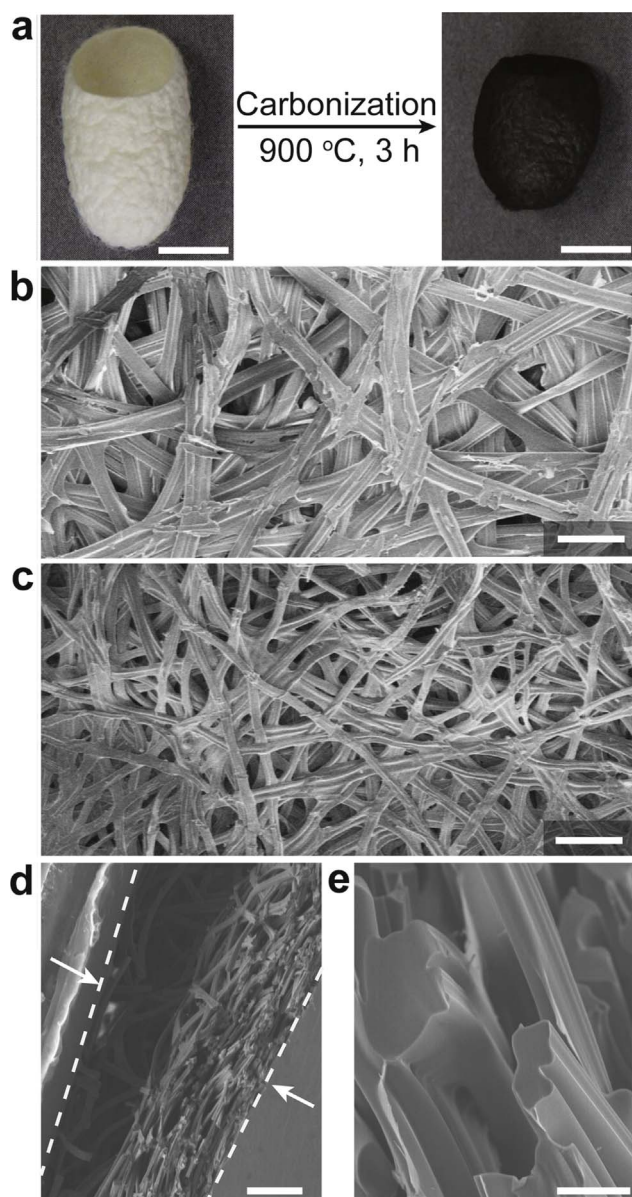


Fig. 1. (a) Schematic presentation of the synthesis of carbonized silk cocoon. (b, c) SEM images of silk cocoon fibers before and after carbonization. (d, e) SEM images of the carbonized silk cocoon under cross-sectional review and corresponding carbonized silk fibers inside under cross-sectional review, respectively. Dashed lines and arrows indicate the area of cross-section in (d). Scale bars are 1 cm for (a), 100 μm for (b, c, and d), and 10 μm for (e).

and fitted with Nova 1.11 (Autolab).

3. Results and discussion

3.1. Characterization of carbonized silk cocoon

The nitrogen-enriched freestanding anode, with 3D and pseudographitic structure, was obtained by direct carbonization of pristine silk cocoon at 900 $^{\circ}\text{C}$ for 3 h under steady N_2 flow, without any pre- or post-treatment (Fig. 1a). Originally, silk cocoon possesses 3D and non-woven structure with piled large pores (Fig. 1b). After carbonization, silk cocoon lost $\sim 80\%$ in weight (Fig. S1), and the fibers shrank from ~ 25 to ~ 10 μm in diameter (Fig. 1b and c). Notably, although raw silk fibers consist of two fibroin brins with sericin conglutination (Fig. S2), after carbonization, the silk fibers fuse into uniform carbon fibers as can be seen in the SEM image (Fig. 1e) [26,27]. Despite the shrinkage, the obtained carbonized silk cocoon

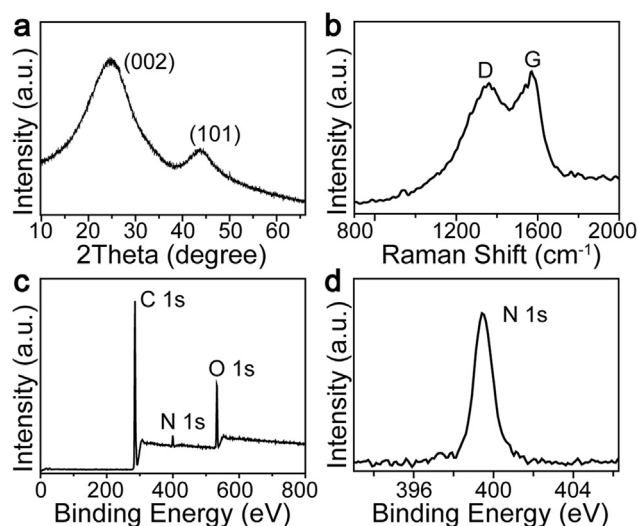


Fig. 2. (a) Powder XRD diffraction pattern, (b) Raman spectrum, (c) XPS survey and (d) high-resolution spectrum of N 1s XPS peak of the carbonized silk cocoon.

maintains its intrinsically 3D non-woven structure with stacked layers and piled macropores (Fig. 1a, c, and d), providing ample space for exoelectrogens (size: ~ 2 μm) to form biofilms and satisfactory reactant/product diffusion after biofilm formation [32,33]. Further N_2 adsorption-desorption studies on carbonized silk cocoon gave a type I/IV adsorption-desorption isothermal curve, with specific surface area of ~ 230 m^2/g (calculated by Brunauer-Emmett-Teller method), indicating the existence of micropores (Fig. S3) [30]. The hierarchical porous structures should be highly suitable to be used as an anode for MFC purposes.

To figure out the structure of the carbonized silk cocoon, we first analyzed it using power X-ray diffraction (XRD). Two peaks, centered at $2\theta=24^{\circ}$ and 44° , were observed in the XRD pattern, indicating its graphitic structure (Fig. 2a) [28,34]. Meanwhile, Raman spectrum of the carbonized silk cocoon showed two characteristic peaks located at ~ 1360 (D band) and ~ 1570 (G band) cm^{-1} , which can be ascribed as distinctive carbon peaks (Fig. 2b). The intensity ratio of G-to-D bands (I_G/I_D) is ~ 1 , revealing the pseudographitic structure (partially graphitized) of the carbonized silk cocoon [28,34]. It should be mentioned that the pseudographitic structure, aromatized from the well aligned β -sheet in silk protein, can provide good conductivity that is highly desired for carbon based MFC anode [34].

We then identified the nitrogen content in the carbonized silk cocoon. The elemental analysis showed a relatively high nitrogen content (6.11 wt%) in the carbonized silk cocoon (Table S1), demonstrating successful creation of N-containing functional groups by protein carbonization, more efficient comparing with other modification methods (Table S1) [9,21,22]. X-ray photoelectron spectroscopy (XPS) studies, on carbonized silk cocoon, confirm the presence of nitrogen species (Fig. 2c, d) from a different point of view. The deconvoluted high-resolution XPS spectrum of N 1s showed a peak centered at 399.4 eV (Fig. S4), indicating the existence of amide/amine groups in the carbonized silk cocoon, which should be preserved from the original protein structures [24,25,35]. In addition, the other peak at 400.3 eV further reveals the presence of pyrrolic/pyridonic N in the carbonized silk cocoon (Fig. S4) [24,25,35]. Taken together, the XRD, Raman, and XPS results suggest that the freestanding carbonized silk cocoon owns pseudographitic structure with nitrogen-enriched contents, and these features could inspire studies in environmental and energy fields, including CO_2 capture [36], flexible capacitors [37], and fuel cell catalysts [38].

3.2. MFC performance

To evaluate the performance of carbonized silk cocoon as a MFC

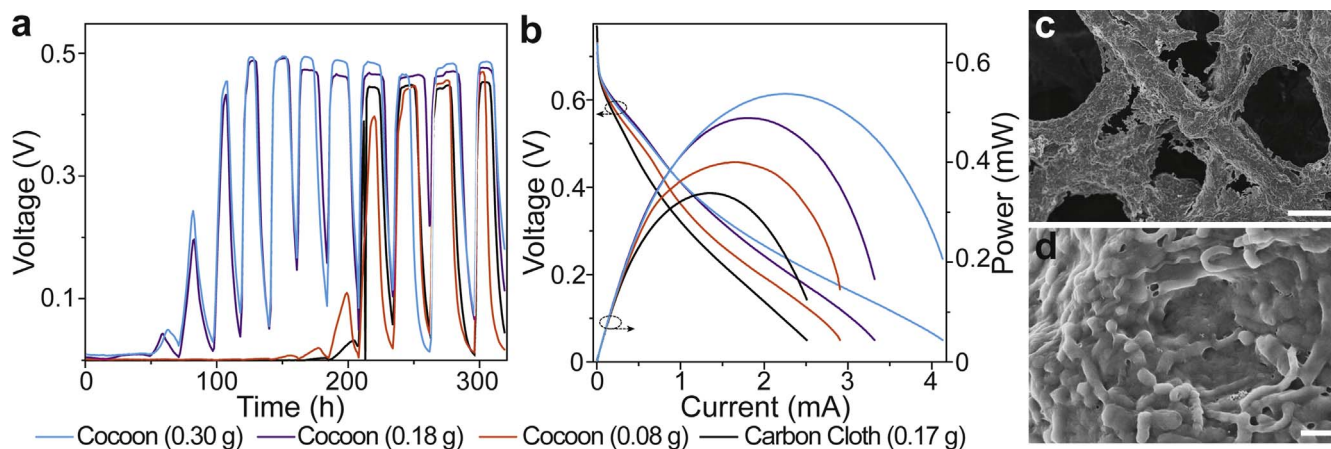


Fig. 3. (a) Time dependent voltage output of MFCs equipped with different anodes in the inoculation stage and running period (external resistance: 1000 Ω). (b) Polarization curves and power curves of MFCs equipped with different anodes obtained by linear sweep voltammetry. Note that Cocoon refers to carbonized silk cocoon anode and dashed arrows in (b) indicate corresponding y axis of the curves. (c, d) SEM images of biofilm grown on a carbonized silk cocoon anode at low and high resolutions, respectively. Scale bars are 20 μm for (c) and 1 μm for (d).

anode, a series of anodes were fabricated by directly stringing the carbonized silk cocoon (weight: 0.08, 0.18 and 0.30 g, respectively) with titanium wire and then incorporated the anodes into single-chamber MFCs (Fig. S5). After inoculated by preacclimated bacteria (originally from activated anaerobic sludge, in which Gram-negative bacteria normally can be the dominant exoelectrogens), the MFCs were fed on artificial wastewater and operated by batch-mode. Intriguingly, the carbonized silk cocoon anode quickly gave a gradually increased cell voltage, where the voltage started to rise from the third cycle (~ 50 h, Fig. 3a). In stark contrast, the MFC, using carbon cloth as an anode with similar weight (0.17 g), operated under the same conditions as a benchmark, began to give voltage output after 8 cycles (~ 190 h). Notably, other than the anode material, the inoculation time of MFCs is also dependent on temperature and bacteria. Particularly, slight change of the preacclimated bacteria may result in large fluctuation of inoculation time. Nevertheless, with repeated experiments, in the same batch, we consistently observed shorter inoculation time of MFCs with carbonized silk cocoon anodes than that of MFCs with carbon cloth anodes.

On a separate note, the carbonized silk cocoon anode, even as light as 0.08 g, had similar inoculation time when compared to that of carbon cloth anode with 0.17 g weight. When MFCs became stable, the voltage output of the MFCs, equipped with carbonized silk cocoon anodes, was relatively higher than that of the corresponding carbon cloth control over 1000 Ω external resistance (Fig. 3a).

Next, the power output of the MFCs was investigated by linear sweep voltammetry at a slow scanning rate of 0.1 mV/s (Fig. 3b). It should be noted that the slow scanning rate was applied in order to minimize the capacitance effect during the measurements [39]. As shown in Fig. 3b, the carbonized silk cocoon anodes yielded similar open circuit voltages ($V_{\text{OCV}} \sim 0.7$ V) to that of a carbon cloth anode, but had higher maximum power outputs and lower internal resistances as indicated by the slope of linear curve region (Table S2). Compared with carbon cloth anode, the carbonized silk cocoon anode (0.08 g) can give a ~ 2.5 -fold maximum gravimetric power density (~ 5.0 mW/g). Moreover, as the weight of the carbonized silk cocoon anode increases, an increase of the maximum power output and a decrease of internal resistance were observed (Table S2). Taking the estimated capital expenditure of carbonized silk cocoon into account, which is $\sim 50\%$ cost of carbon cloth under our conditions (Table S3), we believe that the carbonized silk cocoon anode is more advantageous for future MFC applications.

The reduced inoculation time and improved performance of MFCs when equipped with carbonized silk cocoon anodes, can be firstly attributed to the excellent biocompatibility of carbonized silk cocoon,

as evidenced by the dense biofilm formed on the anode when MFCs became stable (Fig. 3c and d). On the contrary, only scattered biofilm was observed on carbon cloth anode (Fig. S6). Apart from the biocompatibility, the large surface area, macroporous structure and N-containing functional groups of carbonized silk cocoon, which facilitate the attachment of exoelectrogens, should also contribute to the improved performance in MFC. Notably, considering the interaction between bacteria and carbonized silk cocoon anode, we reason that the N-containing functional groups can easily form positively charged quaternary groups and thus can facilitate both the attachment of exoelectrogens, particularly Gram-negative bacteria, and the sequential electron transfer [14,40].

3.3. Electrochemical characteristics of carbonized silk cocoon anode

To gain more insights into the performance of the carbonized silk cocoon anode, cyclic voltammetry was utilized to study the electrochemical activity of different anodes under both turnover (maximum voltage output) and non-turnover (substrate depletion) conditions after successful bacterium inoculation in MFCs (Fig. 4a and b) [41]. It should be mentioned that bare anodes, without exoelectrogens, did not exhibit observable electrochemical redox behaviour (Fig. S7). For carbon cloth anode, after bacterium inoculation, a typical sigmoidal catalyst curve was observed under turnover conditions (Fig. 4a and S8). Meanwhile, two redox peaks, which could be attributed to the redox of outer membrane cytochromes and flavins, respectively, were recorded in the absence of the substrate, indicating the mixed exoelectrogens on anode and extracellular microbial electron transfer during power generation (Fig. 4b and S8) [41].

On the other side, when the carbonized silk cocoon anode with a weight of 0.08 g was used, only a small oxidative peak located at around -0.35 V was observed under turnover conditions (Fig. 4a), which can be attributed to the oxidation of the acetate substrate. While no other obvious redox peak was obtained when MFCs equipped with carbonized silk cocoon anodes at varied weight, under either turnover or non-turnover conditions (Fig. 4a and b). This might be due to the high capacitance of the carbonized silk cocoon, which causes high background current.

To verify the capacitance caused background current on cyclic voltammograms, the anode capacitance was tested by self-charging/discharging method after successful bacterium inoculation (self-charging: 20 min, discharging: 20 min) [42]. As shown in Fig. 4c, when the electric circuit was discharged, MFCs equipped with carbonized silk cocoon anodes gave a transient current peak, with sharp decrease, indicating the release of accumulated charges on the anode [43]. The

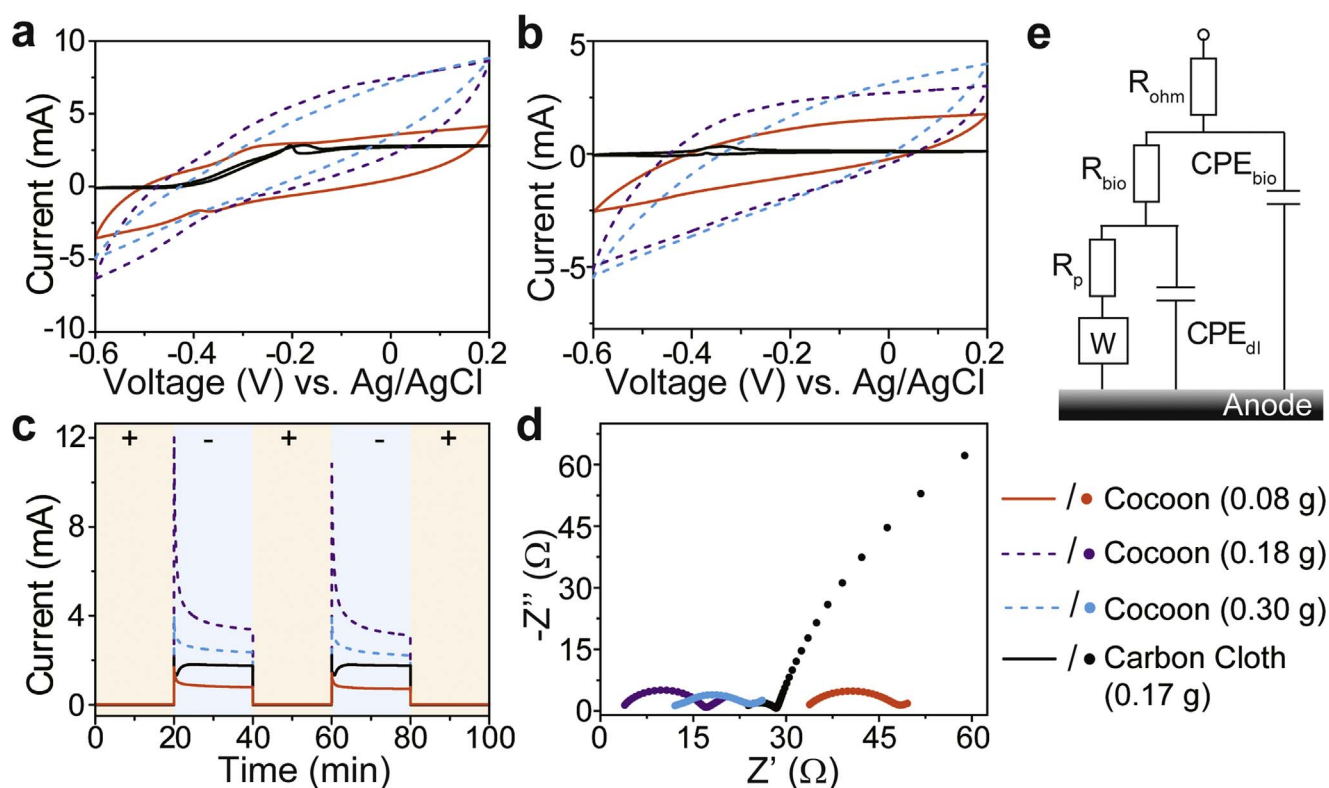


Fig. 4. (a, b) Cyclic voltammograms of the different bioanodes after inoculation under (a) turnover and (b) non-turnover conditions (scan rates: 1 mV/s), respectively. (c) Time dependent current curves of different bioanodes during self-charging/discharging cycles, where + and – represent charging and discharging process, respectively. The anode potential was set at -0.35 V (vs. Ag/AgCl, 3 M KCl electrode) during discharging. (d) Nyquist plots of different bioanodes in MFCs at a three electrode mode. (e) Equivalent circuit for electrochemical impedance spectra fitting. R_{ohm} , R_{bio} , R_p , CPE_{bio} , CPE_{dl} , and W represent ohmic resistance, biofilm resistance, polarization resistance, constant phase element related to biofilm layer, constant phase element related to double layer, and Warburg impedance related to reactant/product diffusion, respectively.

current then gradually decreased and reached a relatively stable value in ~ 20 min. In contrast, a small transient current followed by gradual increase to a steady value was observed in the MFC with the carbon cloth anode, which indicates the absence of anode material discharging. These results together demonstrate the capacitance characteristics of the carbonized silk cocoon. On a separate note, the capacitance of carbonized silk cocoon does not strictly increase linearly with the increase of the weight as indicated by the repeated experiments (Fig. 4c and S9). In addition, it is reasonable that the capacitance effect should contribute to the improved performance of the carbonized silk cocoon anode by other factors, such as increasing the local conductivity and facilitating charge transfer [39,44], although capacitance induced high background current covers some detailed electrochemical information of carbonized silk cocoon anode [45].

Next, electrochemical impedance spectroscopy was employed to study the electron transfer kinetics of both the carbonized silk cocoon anode and carbon cloth anode [46]. The resulting impedance spectra were then plotted as Nyquist curves (Fig. 4d) and analyzed by fitting with equivalent circuit (Fig. 4e) as two arcs in each plot [47,48]. Notably, Warburg impedance, related to the reactant/product diffusion [49], presenting a 45° line in the low frequency range for carbonized silk cocoons while absent in that of carbon cloth, was thus removed from the equivalent circuit in order to give a well matched fitting for the carbon cloth bioanode following the previous report [48].

According to our analysis, carbonized silk cocoon anodes exhibit similar ohmic resistance and biofilm resistance to those of carbon cloth anode. Meanwhile, polarization resistances of the carbonized silk cocoon anode, with varied weight, were estimated to be $\sim 32.5 \Omega$ for 0.08 g, $\sim 5.54 \Omega$ for 0.18 g and $\sim 6.01 \Omega$ for 0.30 g. In stark contrast, the carbon cloth anode exhibited a polarization resistance of $\sim 286 \Omega$, which is one order larger than those of the silk cocoon anodes. Considering the function of the Warburg impedance in our fitting

model, we believe that the carbonized silk cocoon anodes, with high electron transfer rate, could accelerate the reactant consumption and product accumulation during power generation, which could make diffusion a key factor for electrochemical kinetics [50].

3.4. Flexible carbon fiber fabricated MFC anode

Benefited from the featured structure of silk fiber (fibroin@sericin core-shell structure), flexible silk fibers with good mechanical performance can be easily obtained through degumming of silk cocoon by removing sericin using Na_2CO_3 (Fig. S10), which provides promising versatility for silk cocoon to be used for MFC anode fabrication. Subsequently, these flexible silk fibers were carbonized under the same conditions as those of silk cocoon, resulting in flexible carbon fibers, $\sim 5 \mu m$ in diameter, with good mechanical properties (Fig. 5a and b). These flexible carbon fibers then can be used to fabricate flexible MFC anode with predesigned size and shape, including a compact anode for portable and micro-sized MFCs. Notably, as indicated by the XRD data and elemental analysis, the flexible carbon fibers maintained pseudo-graphitic structure and nitrogen-enriched contents, which are similar to those of carbonized silk cocoon (Figs. S12, S13, and Table S1).

As a proof of principle experiment, the flexible carbon fiber anode was directly assembled by twisting titanium wire with the carbon fibers (Fig. S14). Inspiringly, the MFC anode, on the basis of flexible carbon fibers, 0.08 g in weight, showed similar biocompatibility and performance when compared to those of carbonized silk cocoon anode under the same working conditions (Fig. 5c and Table S4). The maximum gravimetric power density of flexible carbon fiber anode is ~ 3.1 time higher than that of carbon cloth anode, and ~ 1.2 times of that of carbonized silk cocoon anode.

Further cyclic voltammetry and self-charging/discharging studies have revealed that the flexible carbon fiber anode also has capacitance

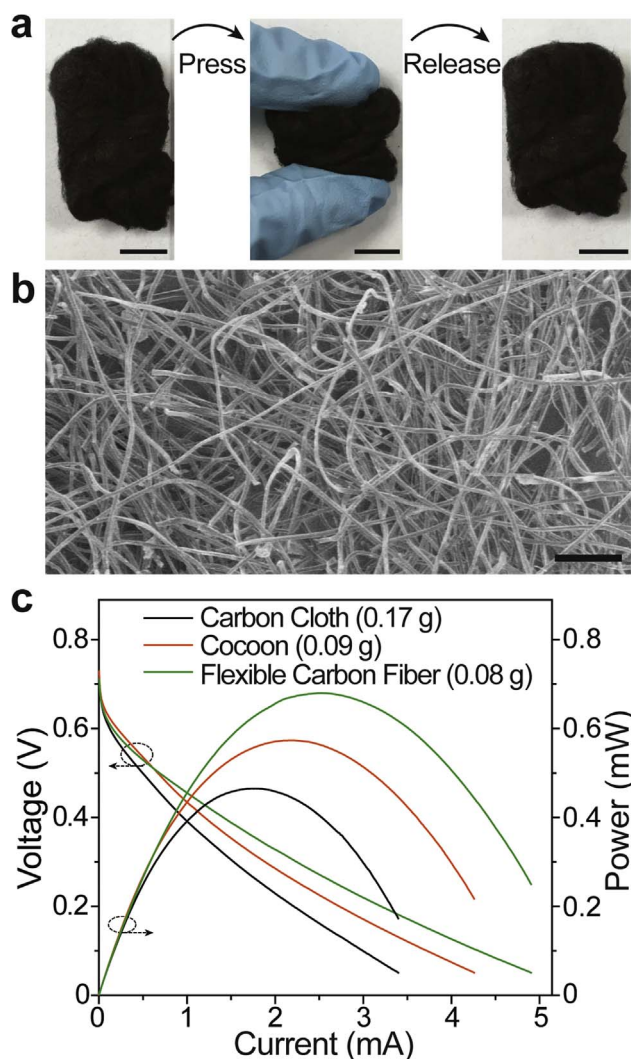


Fig. 5. (a) Digital photographs of flexible carbon fibers pressed by finger tips. (b) SEM image of flexible carbon fibers obtained by carbonization of degummed silk cocoon. (c) Polarization curves and power curves of MFCs equipped with different anodes obtained by linear sweep voltammetry. Note that Cocoon refers to carbonized silk cocoon anode and dashed arrows in (c) indicate corresponding y axis of the curves. Scale bars are 1 cm for (a) and 100 μm for (b).

(Figs. S16 and S17). Electrochemical impedance spectroscopy analysis showed that flexible carbon fiber anode has similar profile to that of carbonized silk cocoon anode, with $\sim 16.3 \Omega$ polarization resistance (Fig. S18). These results indicate carbonized silk cocoon and flexible carbon fiber, are both suitable candidates for MFC anode fabrication. Considering their structure and property difference, freestanding carbonized silk cocoon with rigid structure, could be possibly used outside laboratory, i.e. as stacked or strung anodes in sediment MFCs or as floating anode in marine area, while flexible silk fibers could be strung by current collectors (i.e. stainless steel) into various shapes, versatile for novel MFC designs.

4. Conclusions

The connatural advantages such as enriched nitrogen content, hierarchical 3D microstructure, pseudographitic structure, good biocompatibility and high capacitance, have made the carbonized silk cocoon and its derivatives high performance MFC anode materials, which could help to improve the electron transfer between exoelectrogens and anode. The MFC, equipped with carbonized silk cocoon anodes can offer ~ 2.5 -fold maximum gravimetric power density than

that of MFCs with commonly used carbon cloth anodes. Moreover, flexible carbon fibers can be derived through carbonization of degummed silk cocoon, which allow fabrication of high-performance MFC anodes with varied configurations. The experimental results shown here have demonstrated that the naturally abundant proteins, such as silk cocoon, after direct carbonization, can be a promising material with versatility for high-performance MFC anode fabrication and other electrochemical applications. We believe that the findings shown here should not only provide a new direction for exploring ideal materials as MFC anode, but also inspire other electrochemical applications of natural proteins.

Acknowledgements

We thank L. Nie and J. Wu for SEM and XPS tests. This work was supported by National Natural Science Foundation of China (21401103, 21507059, and 21371095), Natural Science Foundation of Jiangsu Province (BK20150948, BE2015699), Natural Science Foundation for Higher Education Institutions in Jiangsu Province (15KJB150008), Scientific Research Foundation for the Returned Overseas Chinese Scholars, Ministry of Education and Synergetic Innovation Center for Organic Electronics and Information Displays.

Appendix A. Supplementary material

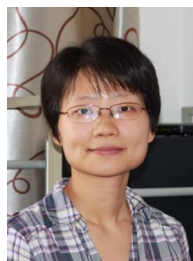
Supplementary data associated with this article can be found in the online version at doi:10.1016/j.nanoen.2016.12.046.

References

- [1] B.E. Logan, K. Rabaey, *Science* 337 (2012) 686–690.
- [2] M. Sun, L. Zhai, W. Li, H. Yu, *Chem. Soc. Rev.* 45 (2016) 2847–2870.
- [3] H. Wang, J. Park, Z. Ren, *Environ. Sci. Technol.* 49 (2015) 3267–3277.
- [4] G. Reguera, K.D. McCarthy, T. Mehta, J.S. Nicoll, M.T. Tuominen, D.R. Lovley, *Nature* 435 (2005) 1098–1101.
- [5] E. Marsili, D.B. Baron, I.D. Shikhare, D. Coursolle, J.A. Gralnick, D.R. Bond, *Proc. Natl. Acad. Sci. USA* 105 (2008) 3968–3973.
- [6] X. Zhang, W. He, L. Ren, J. Stager, P.J. Evans, B.E. Logan, *Bioresour. Technol.* 176 (2015) 23–31.
- [7] G.G. Kumar, V.G.S. Sarathi, K.S. Nahm, *Biosens. Bioelectron.* 43 (2013) 461–475.
- [8] B. Kim, J. An, D. Fapyane, I.S. Chang, *Bioresour. Technol.* 195 (2015) 2–13.
- [9] X. Wang, S. Cheng, Y. Feng, M.D. Merrill, T. Saito, B.E. Logan, *Environ. Sci. Technol.* 43 (2009) 6870–6874.
- [10] D. Pocaznoi, A. Calmet, L. Etcheverry, B. Erable, A. Bergel, *Energy Environ. Sci.* 5 (2012) 9645–9652.
- [11] S.F. Ketep, A. Bergel, A. Calmet, B. Erable, *Energy Environ. Sci.* 7 (2014) 1633–1637.
- [12] R.A. Rozendal, H.V.M. Hamelers, K. Rabaey, J. Keller, C.J.N. Buisman, *Trends Biotechnol.* 26 (2008) 450–459.
- [13] W. Li, H. Yu, Z. He, *Energy Environ. Sci.* 7 (2014) 911–924.
- [14] M. Lu, Y. Qian, L. Huang, X. Xie, W. Huang, *ChemPlusChem* 80 (2015) 1216–1225.
- [15] Y. Yong, X. Dong, M. Chan-Park, H. Song, P. Chen, *ACS Nano* 6 (2012) 2394–2400.
- [16] H. Zhu, H. Wang, Y. Li, W. Bao, Z. Fang, C. Preston, O. Vaaland, Z. Ren, L. Hu, *Nano Energy* 10 (2014) 268–276.
- [17] S. Chen, G. He, A.A. Carmona-Martinez, S. Agarwal, A. Greiner, H. Hou, U. Schröder, *Electrochem. Commun.* 13 (2011) 1026–1029.
- [18] W. Wang, S. You, X. Gong, D. Qi, B.K. Chandran, L. Bi, F. Cui, X. Chen, *Adv. Mater.* 28 (2016) 270–275.
- [19] S. Zhao, Y. Li, H. Yin, Z. Liu, E. Luan, F. Zhao, Z. Tang, S. Liu, *Sci. Adv.* 1 (2015) e1500372.
- [20] Y. Yuan, S. Zhou, Y. Liu, J. Tang, *Environ. Sci. Technol.* 47 (2013) 14525–14532.
- [21] S. Cheng, B.E. Logan, *Electrochem. Commun.* 9 (2007) 492–496.
- [22] J. Liu, J. Liu, W. He, Y. Qu, N. Ren, *J. Power Sources* 265 (2014) 391–396.
- [23] F. Chen, D. Porter, F. Vollrath, *Acta Biomater.* 8 (2012) 2620–2627.
- [24] S.Y. Cho, Y.S. Yun, S. Lee, D. Jang, K.Y. Park, J.K. Kim, B.H. Kim, K. Kang, D.L. Kaplan, H.J. Jin, *Nat. Commun.* 6 (2015) 7145.
- [25] Y.S. Yun, S.Y. Cho, J. Shim, B.H. Kim, S.J. Chang, S.J. Baek, Y.S. Huh, Y. Tak, Y.W. Park, S. Park, H.J. Jin, *Adv. Mater.* 25 (2013) 1993–1998.
- [26] O. Hakimi, D.P. Knight, F. Vollrath, P. Vadgama, *Compos. Part B: Eng.* 38 (2007) 324–337.
- [27] O. Hakimi, D.P. Knight, M.M. Knight, P. Grahn, M.F. Vadgama, *Biomacromolecules* 7 (2006) 2901–2908.
- [28] J. Hou, C. Cao, F. Idrees, X. Ma, *ACS Nano* 9 (2015) 2556–2564.
- [29] S. Cheng, H. Liu, B.E. Logan, *Environ. Sci. Technol.* 40 (2006) 364–369.
- [30] L. Liu, O. Tsyganova, D.J. Lee, A. Su, J.S. Chang, A. Wang, N. Ren, *Int. J. Hydrog.*

Energ. 37 (2012) 15792–15800.

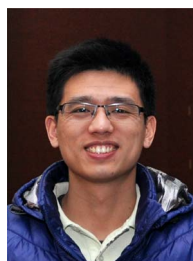
- [31] R.D. Lovley, J.P.E. Phillips, *Appl. Environ. Microb.* 54 (1988) 1472–1480.
- [32] X. Xie, G. Yu, N. Liu, Z. Bao, C.S. Criddle, Y. Cui, *Energy Environ. Sci.* 5 (2012) 6862–6866.
- [33] R. Song, C. Zhao, L. Jiang, E. Abdel-Halim, J. Zhang, J. Zhu, *ACS Appl. Mater. Interfaces* 8 (2016) 16170–16177.
- [34] Z. Li, Z. Xu, X. Tan, H. Wang, C.M.B. Holt, T. Stephenson, B.C. Olsen, D. Mitlin, *Energy Environ. Sci.* 6 (2013) 871–878.
- [35] J.R. Pels, F. Kapteijn, J.A. Moulijn, Q. Zhu, K.M. Thomas, *Carbon* 33 (1995) 1641–1653.
- [36] J.W.F. To, J. He, J. Mei, R. Haghpanah, T. Kurosawa, S. Chen, W.G. Bae, L. Pan, J.B.H. Tok, J. Wilcox, Z. Bao, *J. Am. Chem. Soc.* 138 (2016) 1001–1009.
- [37] D. Liu, G. Cheng, H. Zhao, C. Zeng, D. Qu, L. Xiao, H. Tang, Z. Deng, Y. Li, B. Su, *Nano Energy* 22 (2016) 255–268.
- [38] K. Gong, F. Du, Z. Xia, M. Durstock, L. Dai, *Science* 323 (2009) 760–764.
- [39] C. Feng, Z. Lv, X. Yang, C. Wei, *Phys. Chem. Chem. Phys.* 16 (2014) 10464–10472.
- [40] K. Guo, S. Freguia, P.G. Dennis, X. Chen, B.C. Donose, J. Keller, J.J. Gooding, K. Rabaey, *Environ. Sci. Technol.* 47 (2013) 7563–7570.
- [41] F. Harnisch, S. Freguia, *Chem. -Asian J.* 7 (2012) 466–475.
- [42] J. Tang, Y. Yuan, T. Liu, S. Zhou, *J. Power Sources* 274 (2015) 170–176.
- [43] P.S. Bonanni, G.D. Schrott, L. Robuschi, J.P. Busalmen, *Energy Environ. Sci.* 5 (2012) 6195.
- [44] C. Zhang, P. Liang, Y. Jiang, X. Huang, *J. Power Sources* 273 (2015) 580–583.
- [45] A.J. Bard, L.R. Faulkner, *Electrochemical Methods: Fundamentals and Applications*, John Wiley & Sons, Inc, USA, 2001, pp. 14–18.
- [46] Z. He, F. Mansfeld, *Energy Environ. Sci.* 2 (2009) 215–219.
- [47] X. Dominguez-Benetton, S. Sevda, K. Vanbroekhoven, D. Pant, *Chem. Soc. Rev.* 41 (2012) 7228–7246.
- [48] S. Jung, M.M. Mench, J.M. Regan, *Environ. Sci. Technol.* 45 (2011) 9069–9074.
- [49] X. Peng, H. Yu, X. Wang, N. Gao, L. Geng, L. Ai, *J. Power Sources* 223 (2013) 94–99.
- [50] P.T. Ha, H. Moon, B.H. Kim, H.Y. Ng, I.S. Chang, *Biosens. Bioelectron.* 25 (2010) 1629–1634.



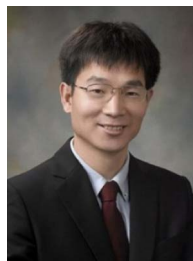
Xiao Huang received her PhD at the School of Materials Science and Engineering of Nanyang Technological University in Singapore in 2011 under the supervision of Prof. Hua Zhang. After that, she worked as a postdoctoral in the same group. She is now a professor at the Institute of Advanced Material (IAM) of Nanjing Tech University in China. Her research interest includes the synthesis and applications of two-dimensional nanomaterial-based hybrid structures.



Hai Li received his BSc from Zhengzhou University, China (2001), and his PhD from the Chinese Academy of Sciences (2007). He was working as a senior research fellow in Prof. Hua Zhang's group from 2008 to 2014 at Nanyang Technological University, Singapore. Then he joined the Institute of Advanced Materials (IAM) in Nanjing Tech University as professor. His research interest includes synthesis, characterization and application of 2D layered nano-materials/ application of micro- & nano- patterning.



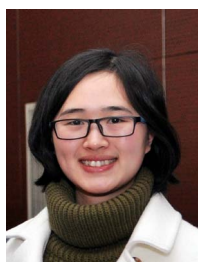
Xiaoji Xie earned his BSc (2009) degree in Chemistry from Nanjing University. He obtained his PhD (2013) at National University of Singapore with Prof. Xiaogang Liu. He then became a postdoctoral researcher working in collaboration with Prof. Xiaogang Liu. He joined the Institute of Advanced Materials (IAM) at Nanjing Tech University (China) in 2014. His current research involves the investigation of inorganic functional nanomaterials for bioapplications, energy harvesting and sensing.



Ling Huang received his PhD from Nanjing University in 2001. After postdoctoral training at University of California at Berkeley, Florida State University, and Northwestern University, he worked as a senior research scientist in the Biomolecular Division of Corning Incorporated, New York, in 2008. He then moved to Nanyang Technological University (Singapore) as an associate professor. In 2012, he joined the Institute of Advanced Materials (IAM) at Nanjing Tech University (China) as a full professor. His current research includes design of lanthanide-doped nanocrystals with novel luminescence and according applications.



Wei Huang received his BSc, MSc and PhD in Chemistry from Peking University in 1983, 1988, and 1992. He became a chair professor at Fudan University in 2012 and was appointed as the Deputy President of Nanjing University of Posts and Telecommunications in 2006. In 2011, he was elected as a member of the Chinese Academy of Sciences (CAS). In 2012, he was appointed as the President of Nanjing Tech University. His current research interests include organic/plastic/flexible electronics, bioelectronics, nanomaterials, nanoelectronics, and polymer chemistry.



Min Lu earned her BSc (2009) degree in chemistry from Nanjing University. She gained her PhD (2014) at National University of Singapore, where she studied cathode catalysts in microbial fuel cells. She joined the Institute of Advanced Materials (IAM) at Nanjing Tech University (China) in 2014. She is currently investigating inorganic nanomaterials for applications in energy and environmental field.



Yijun Qian received his BSc in polymer material and engineering from Nantong University in 2014. He is now a postgraduate student in Institute of Advanced Materials (IAM) at Nanjing Tech University. His current research is focused on improving the performance and energy harvesting efficiency of microbial fuel cells (MFCs).



Cuicui Yang earned her undergraduate degree from Nanjing University in 2012. Currently, she is pursuing her master degree in Institute of Advanced Materials (IAM) at Nanjing Tech University. Her research now is mainly focused on nanomaterial based bioenergy production and wastewater treatment.